Electrical Capacitance Tomography to Measure Moisture Distribution of Polymer Foam in a Microwave Drying Process

Marzieh Hosseini, Anna Kaasinen, Guido Link, Timo Lähivaara, and Marko Vauhkonen

***Abstract*—Moisture distribution information is a critical element in drying processes. The drying of products by employing high-power microwave (MW) technology is widely used in the industry. Although microwaves allow volumetric and selective heating resulting in a significant reduction of processing time and energy consumption, there is always a risk of non-uniform moisture distribution in the final product. This paper investigates the capability of a designed electrical capacitance tomography (ECT) sensor to estimate the moisture distribution of polymer foams in a microwave drying process. The moisture distribution is estimated based on the non-intrusive contactless measurements of the electrical capacitances between the electrodes mounted on a frame around the target polymer foam. The obtained moisture information can be employed as feedback to a controller to adjust the power level of each microwave source in the microwave system to reduce or eliminate the non-homogeneity of the moisture distribution inside the polymer foam. In a series of experiments, we first examine the capability of the ECT sensor in estimating the moisture distribution in a stationary foam. We extend the tests to estimating the moisture distribution in a case where the foam is moving on a conveyor belt. Several study variables are taken, including the sample size, the sample location, the moisture percentage, the conveyor belt speed, and the microwave power. These experiments show that the sensor has a satisfactory accuracy in estimating the moisture distribution of the foam, and the ECT measurements can be further used in a closed-loop control system.**

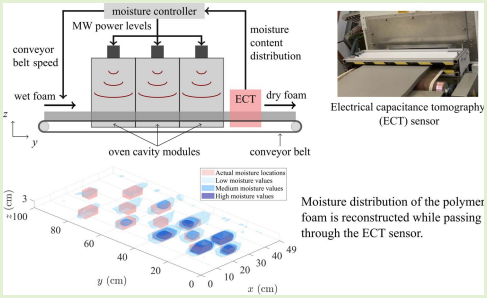

***Index Terms*—Electrical capacitance tomography, moisture measurements, microwave drying.**

I. Introduction

DRYING processes have many industrial applications, for example, in food preservation and wood processing. Among different drying technologies, such as conventional heating, where there is an external heating source, microwave drying is becoming an attractive candidate for drying high moisture materials [1]–[3]. Volumetric and selective heating in microwave drying results in the fast internal evaporation of moisture. In this process, the wet material is exposed to several microwave sources in an oven cavity until the water inside the material evaporates.

One of the main goals of microwave drying technology is to achieve as uniform moisture distribution inside the material as possible since it has a high impact on the final product quality. Typically, the aim is to reach a certain level of moisture in the dried material. Designing an advanced moisture controller for the microwave drying process can help to reach a homogenous moisture distribution. Such kind of controller has not been designed for drying processes since it needs in situ information about the moisture distribution of the material.

As one of the traditional methods, the temperature of the material is monitored to control the drying process [4]–[7]. In [4], [6], [7], the authors used the temperature measurement from one point on the sample to control the drying temperature by adjusting the microwave power. Authors in [5] employed

Manuscript received March 12, 2021; revised April 28, 2021; accepted May 20, 2021. Date of publication June 3, 2021; date of current version August 13, 2021. This work was supported in part by the European Union's Horizon 2020 Research and Innovation Programme through the Marie Skłodowska-Curie Grant under Agreement 764902 and in part by the Academy of Finland (Finnish Centre of Excellence of Inverse Modelling and Imaging) under Project 312344 and Project 321761. The associate editor coordinating the review of this article and approving it for publication was Prof. Chao Tan. *(Corresponding author: Marzieh Hosseini.)*

Marzieh Hosseini, Anna Kaasinen, Timo Lähivaara, and Marko Vauhkonen are with the Department of Applied Physics, University of Eastern Finland, 70210 Kuopio, Finland (e-mail: marzieh.hosseini@uef.fi; anna.kaasinen@uef.fi; timo.lahivaara@uef.fi; marko.vauhkonen@uef.fi).

Guido Link is with the Institute for Pulsed Power and Microwave Technology, Karlsruhe Institute of Technology, 76131 Karlsruhe, Germany (e-mail: guido.link@kit.edu).

Digital Object Identifier 10.1109/JSEN.2021.3085762

infrared thermography to identify the instant hot spots on the samples rather than monitoring the temperature of one fixed position. However, temperature control can only prevent overheating, and the temperature distribution does not necessarily correspond with the moisture distribution. Therefore, this method is insufficient for having a homogenous moisture distribution.

The moisture distribution can only be obtained using tomographic sensors. In general, the benefits of combining process tomography with a feedback controller have been widely recognized [8], [9], and the idea has been tested with simulations [10]. Recently, microwave tomography has been studied to estimate the moisture distribution in a simulated microwave drying process [11]. However, tomographic sensors have not been used yet in monitoring the moisture distribution in microwave drying processes. The most practiced method of measuring the moisture content in this process is by measuring the sample weight during or after the process [12]–[17]. In most cases, like in [12], the authors attached the sample to a digital balance by a hook and recorded the sample weight loss during the drying process. This method can only give the average moisture of the material. Moreover, it is impossible to use this method for larger samples or in continuous processes where the wet material moves through the oven cavity.

Electrical capacitance tomography (ECT) has shown to be an attractive tool for monitoring moisture distribution in several applications since it is non-intrusive, non-invasive, and inexpensive [18]–[23]. In [20], the author employed the ECT sensor in imaging three-dimensional (3D) unsaturated moisture flow in cement-based materials. The ECT sensor consisted of several electrode plates to make 3D imaging possible. In [23], the authors used the ECT sensor designed with eight electrodes on one plate rounded around woody biomass samples to estimate their moisture content. They compared the results with the near-infrared spectroscopy method to find the best way to estimate the moisture content of the samples.

One of the microwave drying process applications is the drying of polymer foams in the heat insulation industry. In this process, it is essential to dry the foam below a certain level (e.g., 15-20% on a wet basis), and the remaining moisture should have as homogenous distribution as possible. If some parts of the foam dry while other parts are still wet, the product can be damaged due to overheating or burning. The overheating of the foam can also destroy the whole microwave system and the production line. This paper aims to design an ECT sensor to estimate the moisture distribution of polymer foams in a continuous microwave drying process. The ECT sensor measures the contact-free capacitances between the electrodes mounted on a frame around the foam. The measurements are then employed in a reconstruction algorithm to estimate the foam permittivity distribution. Since the material permittivity strongly correlates with the material moisture, a calibration curve between the estimated permittivity and the actual moisture of the material is determined to estimate the moisture distribution. The moisture estimates can further be integrated into a closed-loop controller to counteract an inhomogeneous moisture distribution in the foam.

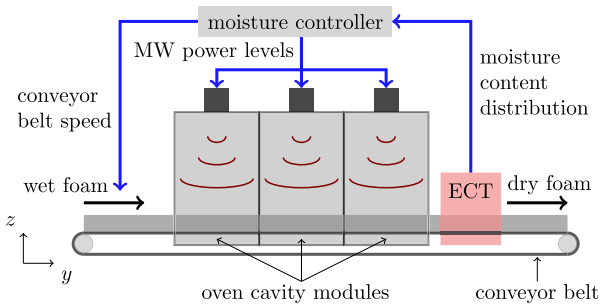

Fig. 1. A schematic picture of the microwave drying process employed in this study.

Even though the basic principles of how an ECT sensor works are the same for any application, the designs can be completely different. Each application requires its specifications regarding the frame size, the number of the electrodes, the electrode size, and the electrode locations. Each of these factors can highly affect the reconstruction results. In this paper, an ECT sensor is developed based on the most efficient design according to the simulations and experiments to estimate the moisture distribution of moving polymer foams. The application has some unique requirements considered in the sensor design, such as the mobility of the material and its large size, which results in very low measured electrical capacitances between most of the electrodes. The ECT measurements are fast, and they can be used in in-line, real-time measurements. In this paper, the performance of the ECT in the case of stationary and moving foams is evaluated through a series of experiments.

II. Microwave Drying Process

The microwave drying process has been an attractive technology during the past decades by demonstrating time and energy efficiency in many applications. Figure 1 illustrates a schematic picture of the microwave drying system considered in this study with three oven cavity modules, each equipped with six 2 kW, 2.45 GHz microwave sources distributed on the hexagonal sides of the oven. This system is a combination oven with convective heating, which allows the transport of the evaporated moisture out of the system.

The microwave drying technology is associated with the dielectric heating of poorly conductive products such as polymer foams, the test material in this study. In the heat insulation industry, the impregnation of polymer foams introduces new features to the foam by dipping it into a bath, squeezing it, and then drying it by passing it through an oven. The squeezing step is designed to ensure the most homogenous moisture distribution inside the foam at the beginning of the drying process. After the impregnation process, the wet foam enters the oven on a conveyor belt, passes through the oven cavity modules, and exits from the other side of the system. Figure 2 shows a schematic of a cross-section of one of the cavity modules.

The infrared cameras installed in each module can monitor the surface temperature distribution of the foam throughout

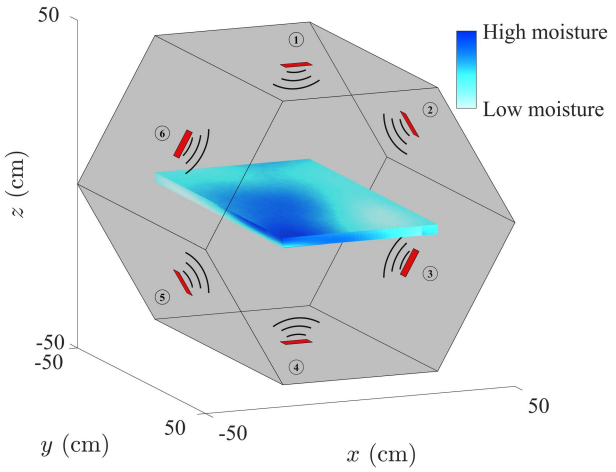

Fig. 2. A cross section of a microwave oven module.

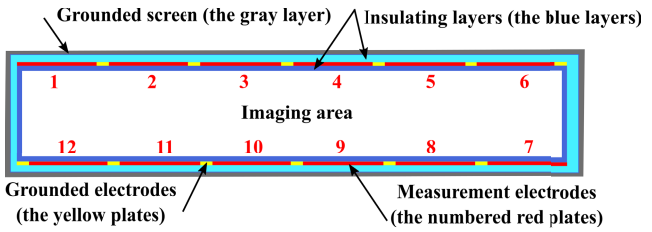

Fig. 3. An illustration of the ECT sensor: The target material (foam) is placed in the imaging area. Measurement electrodes are mounted around the foam. There is an electrically grounded electrode between adjacent measurement electrodes to improve the sensitivity of their measurements. An electrically grounded metal screen is surrounding the electrode plates to reduce the background noise. Also, the electrode plates are separated from the metal screen and the imaging area by insulating layers.

the drying process. However, there is no available information on the moisture distribution of the foam during and after the process. So far, no sensor for monitoring the moisture distribution of the drying material has been designed for this process.

In this study, an ECT sensor is developed to estimate the moisture distribution of polymer foams right after the drying process. For safety reasons, the ECT sensor cannot be placed inside the microwave oven. The information obtained from the sensor will be an essential part of the moisture control unit [24].

III. Electrical Capacitance Tomography

Electrical capacitance tomography is an imaging sensor employed to reconstruct the material permittivity, which strongly correlates with the moisture distribution inside the material.

The ECT device works based on inter-electrode capacitance measurements between the electrodes mounted on a frame around the target material. Figure 3 shows an illustration of the ECT sensor. The measurement procedure involves applying an electrical voltage to excite one of the measurement electrodes while the rest are grounded. The electrical capacitance between the exciting electrode and the other grounded ones is measured, and then the same operation is repeated to other measurement electrodes. It should be noted that there is a narrow electrically grounded electrode installed between every adjacent measurement electrodes to improve the sensitivity of the measurements. However, they are not involved in the measurement procedure, and the electrical capacitance is only measured between the measurement electrodes. By having N_{el} measurement electrodes, $m = N_{\text{el}}\left(N_{\text{el}}-1\right)/2$ measurements are gathered in each frame. Based on the obtained measurements, the permittivity distribution is reconstructed.

To solve the reconstruction problem, which is also referred to as the inverse problem, we need to solve the forward problem first. The forward problem formulates a model to connect the ECT measurements, the electric potential distribution, and the permittivity distribution. In our study, the forward model is adopted from the complete electrode model, which has different boundary conditions than the conventional ECT model. The complete electrode model takes the electrode model into account more accurately. It has been developed first for the electrical impedance tomography [25] and then derived for the ECT [26].

Let $\mathbf{x} \in \Omega$ denote the spatial coordinate in the computational domain Ω. The permittivity $\epsilon(\mathbf{x})$ can be defined as

$$\epsilon(\mathbf{x}) = \epsilon_0 \epsilon_{\text{r}}(\mathbf{x}), \tag{1}$$

where $\epsilon_0 \approx 8.8542 \times 10^{-12}$ Fm^{-1} is the vacuum permittivity, and $\epsilon_{\text{r}}(\mathbf{x}) \geq 1$ is the relative permittivity of the material. The complete electrode model for ECT can be written as

$$\nabla \cdot (\epsilon(\mathbf{x}) \nabla u(\mathbf{x})) = 0, \quad \mathbf{x} \in \Omega, \tag{2}$$

with the boundary conditions

$$u(\mathbf{x}) + \zeta_l \epsilon(\mathbf{x}) \frac{\partial u(\mathbf{x})}{\partial \nu} = U_l, \quad \mathbf{x} \in \partial\Omega_{\text{el}}^{(l)}, \ l = 1, \ldots, N_{\text{el}} \tag{3}$$

$$\int_{\partial\Omega_{\text{el}}^{(l)}} \epsilon(\mathbf{x}) \frac{\partial u(\mathbf{x})}{\partial \nu} dS = q_l, \quad l = 1, \ldots, N_{\text{el}} \tag{4}$$

$$\frac{\partial u(\mathbf{x})}{\partial \nu} = 0, \quad \mathbf{x} \in \partial\Omega \setminus \partial\Omega_{\text{el}}, \tag{5}$$

where N_{el} is the total number of measuring and grounded electrodes, ν is the outward unit normal vector of the electrode surface or the target boundary, $u(\mathbf{x})$ is the electric potential distribution, ζ_l is a small coefficient modeling an almost negligible potential drop on the electrodes, U_l is the applied potential on the l-th electrode, q_l is the unknown electric charge on the l-th electrode, and $\partial\Omega_{\text{el}} = \cup_{l=1}^{N_{\text{el}}} \partial\Omega_{\text{el}}^{(l)}$ is the union of the electrode surfaces. Based on experimental tests [26], the parameter ζ_l is taken as $\zeta_l = \zeta = 10^{-9}$, $l = 1, \ldots, N_{\text{el}}$.

The forward model is numerically solved using the finite element method [26], [27]. By augmenting the models corresponding to a set of m measurements in a vector and assuming additive measurement noise, the observation model for ECT can be formulated as

$$\boldsymbol{C} = \mathcal{H}(\boldsymbol{\epsilon}) + \boldsymbol{v}, \tag{6}$$

where $\boldsymbol{C} = [C_1, \ldots, C_m]^T$ denotes the vector of the measured electrical capacitances between the electrodes,

$\boldsymbol{\epsilon} = [\epsilon_1, \ldots, \epsilon_n]^T$ is the discretized permittivity distribution, n is the number of the discretization points, $\mathcal{H}(\boldsymbol{\epsilon}) = [h_1(\boldsymbol{\epsilon}), \ldots, h_m(\boldsymbol{\epsilon})]^T$ is the map between the permittivity distribution, $\boldsymbol{\epsilon}$, and capacitances, $\boldsymbol{C}$, resulting from the finite element (FE) approximation, and $\boldsymbol{v} = [v_1, \ldots, v_m]^T$ is the additive measurement noise.

The forward model of ECT connects the measured electrical capacitances with the permittivity distribution and is mathematically a well-posed problem. However, the inverse problem is an ill-posed problem that aims to reconstruct the permittivity distribution based on the capacitance measurements. There are many techniques proposed to solve the inverse problem of ECT [28]–[31]. Some methods have the capability of finding the absolute value of the permittivity. However, they are usually computationally expensive and slow. In this study, the difference imaging method is employed to reconstruct the permittivity changes of the wet material compared to the permittivity of the dry material. The chosen technique is a linear method; therefore, it is computationally fast and suitable for real-time measurements. However, due to the approximation error of the linearization, there can be a relatively high estimation error for the permittivity change value when using the difference imaging method. This drawback can be overcome in our application by using a calibration curve between the estimated permittivity and the actual material moisture.

In the difference imaging method, the observation model (6) is approximated by the first-order Taylor polynomial as

$$\boldsymbol{C} \approx \mathcal{H}\left(\boldsymbol{\epsilon}^*\right) + \boldsymbol{J}\left(\boldsymbol{\epsilon}^*\right)\left(\boldsymbol{\epsilon} - \boldsymbol{\epsilon}^*\right) + \boldsymbol{v}, \tag{7}$$

where $\boldsymbol{J}\left(\boldsymbol{\epsilon}^*\right) = \partial \mathcal{H}\left(\boldsymbol{\epsilon}^*\right)/\partial \boldsymbol{\epsilon}$ is the Jacobian matrix [26], and $\boldsymbol{\epsilon}^*$ is the linearization point. Two sets of measurements are collected: $\boldsymbol{C}_{\text{ref}}$, which denotes the measurements before the change in the permittivity (the measurements of the dry material), and $\boldsymbol{C}_{\text{M}}$, the measurements after the permittivity change (the measurements of the wet material). With these measurements, the approximated model for the difference data $\Delta \boldsymbol{C} = \boldsymbol{C}_{\text{M}} - \boldsymbol{C}_{\text{ref}}$ can be computed as

$$\Delta \boldsymbol{C} = \boldsymbol{J} \Delta \boldsymbol{\epsilon} + \Delta \boldsymbol{v}, \tag{8}$$

where $\Delta \boldsymbol{\epsilon} = \boldsymbol{\epsilon} - \boldsymbol{\epsilon}_{\text{ref}}$ is the change in the permittivity compared to the dry material permittivity, $\boldsymbol{\epsilon}_{\text{ref}}$, and $\Delta \boldsymbol{v}$ is the change of the noise term.

The permittivity change $\Delta \boldsymbol{\epsilon}$ can be estimated using the Bayesian framework leading to the optimization problem [32]

$$\widehat{\Delta \boldsymbol{\epsilon}} = \arg\min_{\Delta \boldsymbol{\epsilon}} \left\{ ||L_{\Delta \boldsymbol{v}} \left(\Delta \boldsymbol{C} - \boldsymbol{J} \Delta \boldsymbol{\epsilon}\right)||^2 + ||L_{\Delta \boldsymbol{\epsilon}} \Delta \boldsymbol{\epsilon}||^2 \right\}, \tag{9}$$

where $L_{\Delta \boldsymbol{v}}^T L_{\Delta \boldsymbol{v}} = \Gamma_{\Delta \boldsymbol{v}}^{-1}$ and $\Gamma_{\Delta \boldsymbol{v}}$, the covariance matrix of the measurement noise term $\Delta \boldsymbol{v}$, is computed as $\Gamma_{\Delta \boldsymbol{v}} = 2\Gamma_{\boldsymbol{v}}$, where $\Gamma_{\boldsymbol{v}}$ is the covariance matrix of the measurement noise $\boldsymbol{v}$. Moreover, $L_{\Delta \boldsymbol{\epsilon}}$ is a smoothness promoting prior, calculated through the Cholesky factorization as calculated in [33]. Eventually, the difference imaging solution can be calculated as

$$\Delta \boldsymbol{\epsilon} = K\left(\boldsymbol{C}_{\mathbf{M}} - \boldsymbol{C}_{\text{ref}}\right), \tag{10}$$

Fig. 4. Polymer foam samples with the thickness of 30 mm.

where K is the reconstruction matrix and is calculated as [32]

$$K = \left(\boldsymbol{J}^T \Gamma_{\Delta \boldsymbol{v}}^{-1} \boldsymbol{J} + \Gamma_{\Delta \boldsymbol{\epsilon}}^{-1}\right)^{-1} \boldsymbol{J}^T \Gamma_{\Delta \boldsymbol{v}}^{-1}. \tag{11}$$

Equation (10) calculates the permittivity change distribution of the material. The calibration curve between the estimated permittivity change and the actual moisture of the foam can be used afterward to calculate the estimates of the moisture distribution. The calibration curve is obtained in this paper using the experimental data.

IV. Materials and Methods

The capability of the ECT sensor when estimating the moisture distribution of polymer foams is investigated in this study through several experiments. In the following sections, the devices, materials, and experimental procedures are described in detail.

A. Samples

Polymer foams have many applications in the heat insulation industry, such as sealing tapes of windows. In this study, we used raw polymer foams with a density of 23 ± 2 kg/m^3. The foam width was 493 mm, and it had a thickness of 30 mm. The studied process is continuous; however, a limited length of the foam was used in our experiments. Figure 4 shows three samples of this polymer foam.

B. ECT Device

The measurement procedure and the theory behind the ECT were explained in Section III. Several factors in designing the ECT sensor can considerably affect the reconstruction accuracy and the sensor spatial resolution. In our application, the ECT sensor and consequently the 2D image of the cross-section were rectangular, while most common ECT setups are round. Moreover, the large width of the foam required a wide structure for the ECT which resulted in a considerable distance between the non-neighboring electrodes. Therefore, only a few measurements were large enough to affect the reconstructions. This issue made the permittivity distribution reconstructions challenging and required a sensor design to address the practical limitations and reduce their effects on the measurement signal.

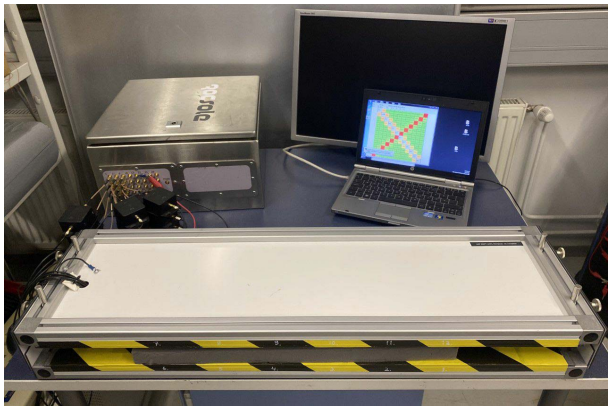

Fig. 5. The ECT sensor while measuring the inter-electrode capacitances. A dry polymer foam is placed inside the sensor.

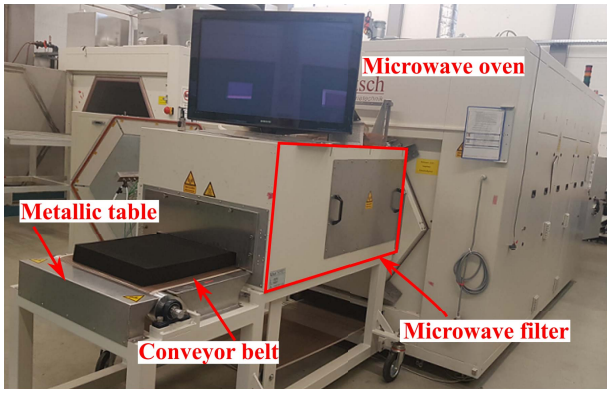

Fig. 6. A picture of the HEPHAISTOS microwave system located at KIT, Germany.

In designing the ECT sensor, it was essential to have the electrodes on both the top and bottom surface of the foam. The simulation results predicted that the moisture on the bottom parts of the foam could not be detected without the electrodes on the bottom surface. Therefore, modifying the metallic table on which the conveyor belt was moving was required since the table prevented transmitting any signal from the bottom electrodes. Furthermore, since the thickness of the foam was only 30 mm, no electrodes were needed on the sides of the ECT sensor. The design of the developed ECT sensor is similar to the illustration shown in Fig. 3.

The dimension of the sensor structure was 870 mm × 250 mm × 40 mm. The height of the sensor was adjustable as the foam thickness can be different in future studies. Six measurement electrodes were mounted on the top surface and another six measurement electrodes on the bottom surface of the ECT sensor. Each measurement electrode was 100 mm × 81 mm, and the electrically grounded electrodes between every adjacent measurement electrodes were of the size of 100 mm × 3 mm. A thin electrically grounded aluminum shield was covering the sensor structure to reduce the background noise. Furthermore, the electrode plane was separated from the metal shield and foam with insulating layers.

Since the foam was moving through the sensor, there was an air gap of 10 mm between the foam and the electrodes on the top surface of the sensor. The ECT sensor can conduct contact-free imaging; however, the air gap required for the foam movement increased the distances between the electrodes and the foam, which could degrade the ECT signal. In our design, we overcame this problem by considering a large width for the measurement electrodes, improving the measurement signal. Figure 5 shows the designed and built ECT sensor to be installed at the microwave exit.

The sensor was connected to a measurement device built by Rocsole Ltd., Kuopio, Finland. The measurement device applied AC voltage with the magnitude of 2.5 V and frequency of 625 kHz to the exciting electrodes and measured the inter-electrode capacitances. The frequency resulting in the best reconstruction was determined based on experimental results, and the voltage magnitude was chosen automatically by the measurement device. The measurements were transferred in real-time to a laptop connected to the device. Each frame of the measurements took less than a second. The measured electrical capacitances were used in the difference imaging algorithm to reconstruct the permittivity distribution of the foam.

The reconstruction algorithm computes the 2D permittivity distribution of the material. In 2D reconstruction, it is assumed that the permittivity in the y-direction, which is the foam moving direction, is constant, and the permittivity distribution is reconstructed in only a cross-section of the foam. The FE mesh representing the reconstructed permittivity in this study has a density of 824 nodes with 1430 elements, which provides enough spatial resolution considering our application.

C. Microwave Drying System

Our testbed system is called HEPHAISTOS, a large-scale microwave oven located at Karlsruhe Institute of Technology (KIT), Germany. The oven includes three cavity modules, each 100 cm in length, as explained in Section II. Since the system is an open oven, two microwave filters, each 150 cm in length, are installed at both sides of the oven to block the microwave power leakage from the entering and exit points. The whole length of the system is 729 cm.

A picture of this device is shown in Fig. 6. The system is operated by software named SIMPAC developed by the manufacturing company of the microwave system, Vötsch Industrietechnik GmbH, Germany. The microwave sources are the sources of heating energy, which result in the evaporation of the foam moisture. Moreover, there is hot air circulating in the device to remove the evaporated moisture. The power levels of the microwave sources, the hot air temperature, and the conveyor belt speed can be controlled using SIMPAC.

D. Experiments

1) Stationary Measurements: In the first set of experiments, a stationary case was studied. In this test, a board of foam with a dimension of 493 mm × 250 mm × 30 mm was inserted inside the sensor. The purpose of this experiment was to identify the wet parts of the foam. Three pieces denoted as P1, P2, and P3, of the foam, were cut, moisturized up to

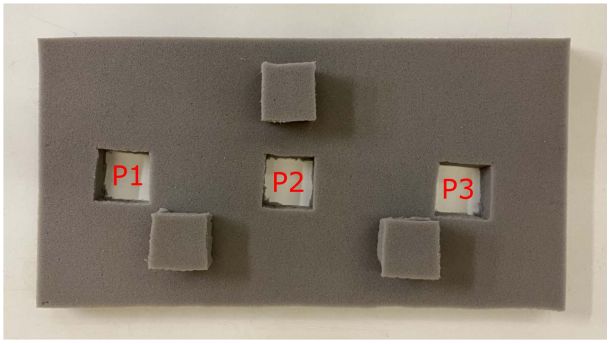

Fig. 7. The sample foam for the stationary measurements with three separate moisture locations.

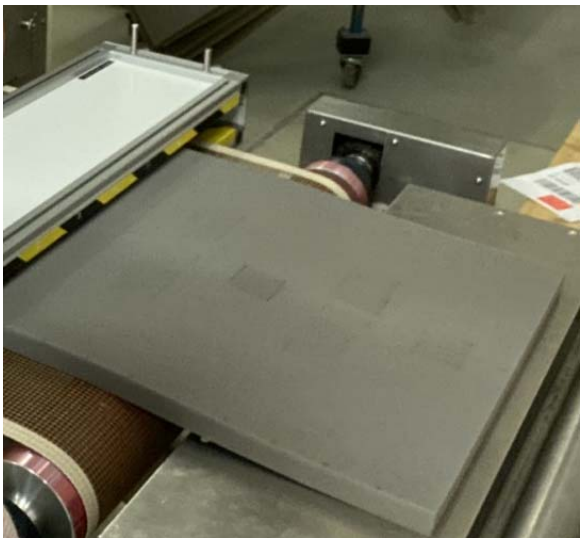

Fig. 8. The ECT sensor installed on the microwave system while measuring the moisture distribution of a moving foam sample.

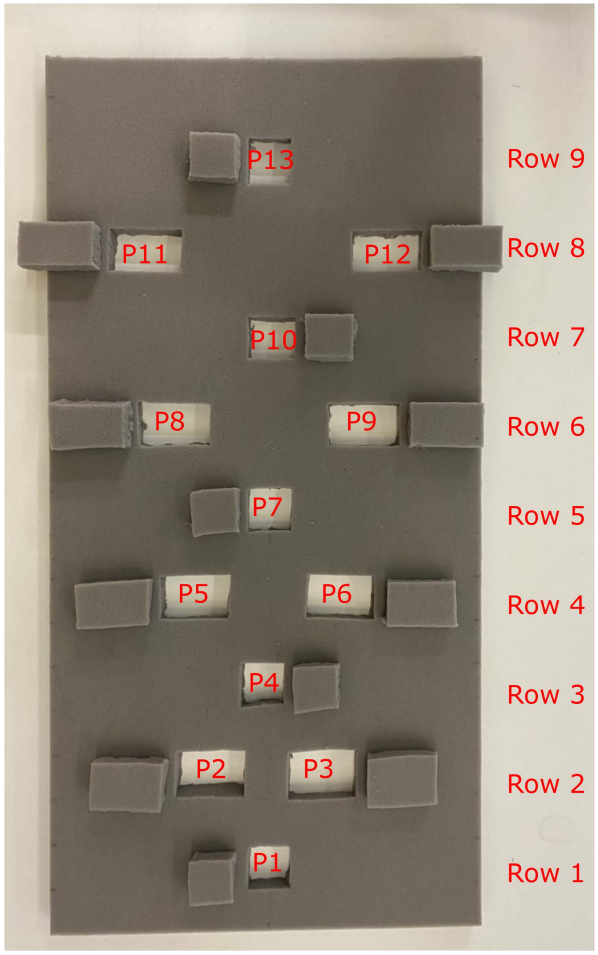

Fig. 9. The sample foam for the dynamic measurements (moving foam) with 13 separate moisture locations.

a certain amount, and returned to their original locations to validate the results. Figure 7 shows a picture of the foam, which includes the three wet pieces. All pieces were cut in the same size of 50 mm × 50 mm × 30 mm and arranged at an equal distance. The first and the third piece also had the same distance from the left and right sides of the foam. The moisture distribution of the foam was estimated in three different experiments. These experiments were conducted to evaluate the sensor sensitivity to the moisture level and its accuracy in identifying the moisture locations.

In the first experiment, P1 had more moisture than the other two pieces. In the second experiment, the moisture content of P2 was increased to almost the same level as P1, while P3 had the lowest moisture level. Finally, in the third experiment, all pieces were wet with the same amount of moisture. The weight of every piece was measured both while dry and after adding the water to compute the actual moisture percentage. The wet basis moisture percentage was calculated as

$$M = \frac{W_{\mathrm{w}} - W_{\mathrm{d}}}{W_{\mathrm{w}}} \times 100, \tag{12}$$

where W_{d} is the weight of the dry piece and W_{w} is the weight of the same piece after adding the water.

2) Dynamic Measurements: After evaluating the sensor performance in the stationary measurements, the sensor was installed on the microwave system right after the microwave filter on the exit point. The following experiments aimed to measure the moisture distribution of a polymer foam while passing through the sensor on a conveyor belt. Figure 8 shows the ECT sensor while measuring the electrical capacitances as the foam was moving through the sensor. The sample foam for this experiment was of a dimension of 493 mm × 1000 mm × 30 mm. It contained 13 different pieces, which were cut, moisturized, and returned to their original locations in nine rows. Figure 9 shows this board of foam, while the nine rows are indicated in the picture. The size, location, and moisture content of the pieces in this sample foam were chosen such that several factors can be studied throughout the experiments.

Three different experiments were conducted with the moving foam to study the effects of the belt speed and the microwaves on the reconstructions. In the microwave drying of polymer foams, the conveyor belt speed can be chosen from 20 cm/min to 40 cm/min. In the first experiment, the microwave power sources were off, and the foam was wet with the known moisture amounts before passing through the sensor. The belt speed in this experiment was 40 cm/min. Since the ECT sensor should be able to work while the microwave

sources are on, the second experiment was done with the same belt speed while the microwave sources were working. The third experiment was conducted with a 20 cm/min belt speed while the microwave sources were off.

3) Moisture Calibration: In the microwave drying process, the goal is to determine the moisture distribution of the drying material. However, the difference imaging method only estimates the change in the permittivity distribution, which is correlated to the moisture. A mapping between the estimated permittivity changes calculated from (10) and the actual moisture values was determined to calculate the moisture distribution of the foam.

In both stationary and dynamic experiments, the actual wet basis moisture percentage of the pieces was computed from (12). Let M_i, $i = 1, 2, 3$ be the actual moisture percentage of the i-th piece in one of the stationary experiments. The estimated permittivity change distribution in this experiment was calculated using (10). This distribution can be employed to compute the dry basis permittivity change (in percentage), $\Delta\epsilon_{\mathrm{d}}$, as

$$\Delta\epsilon_{\mathrm{d}} = \frac{\Delta\epsilon}{\epsilon_{\mathrm{ref}}} \times 100, \tag{13}$$

where ϵ_{ref} is the best homogeneous estimate of the dry foam permittivity. It is assumed that the dry foam has a homogenous permittivity distribution, so only one value was estimated for the whole permittivity distribution. Since the wet basis was used to compute the moisture percentage in our application, the dry basis permittivity change was converted to the wet basis permittivity change, $\Delta\epsilon_{\mathrm{w}}$ (in percentage), before determining the mapping. The dry and wet basis permittivity change are related as

$$\Delta\epsilon_{\mathrm{w}} = \frac{\Delta\epsilon_{\mathrm{d}}}{100 + \Delta\epsilon_{\mathrm{d}}} \times 100. \tag{14}$$

As only the average moisture percentage of each piece was known, instead of using the whole permittivity distribution, the average value of $\Delta\epsilon_{\mathrm{w}}$ in the corresponding area to the i-th piece, referred to as $\Delta\epsilon_{\mathrm{w},i}$, was calculated. A mapping between the $\Delta\epsilon_{\mathrm{w},i}$ and M_i was found using the data obtained from different stationary experiments with various moisture percentages for every piece. The calculated mapping was used to transform the estimated permittivity distribution of the foam to the moisture distribution in the stationary experiments. The same procedure was followed for the dynamic experiments to map the estimated permittivity change and the actual moisture when the foam was moving. The foam movement and the long length of the sample foam in the dynamic experiments resulted in different reconstructed permittivity values than the stationary experiment. Therefore, the same calibration as in the stationary experiments could not be used in the dynamic experiments but required a different calibration.

V. Results and Discussions

A. Reconstruction Results of the Stationary Measurements

Three different experiments were conducted in the stationary measurements where a board of foam with three moisture locations was placed inside the ECT sensor. As noted in Section II, the difference imaging method requires the electrical capacitance measurements of both the dry and wet foams. Figure 10 displays the measured capacitances of the wet and the dry foams in Experiment 1 of the stationary experiments. Here, the electrical capacitance of the wet foam in some measurements is larger than in the dry foam measurements due to the increased moisture level near the corresponding electrode plates. Moreover, as mentioned in Section IV-B, because of the rectangular structure of the ECT sensor and its large width, only 26 out of 66 measurements are adequately large, which can be seen as the peaks in Fig. 10. The peaks in both measurement sets correspond to the neighboring or opposing electrodes, and the rest of the measurements are close to zero. Therefore, effectively the reconstructions were calculated based on the 26 highest measurements.

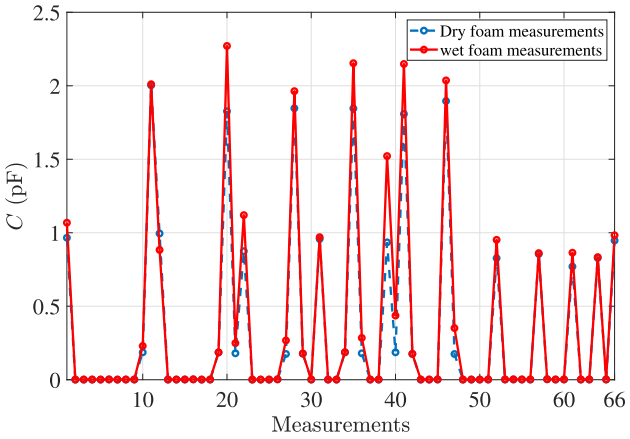

Fig. 10. The wet and dry foam measurement data in the Experiment 1 of the stationary experiments.

Based on the reconstruction results of these experiments, a calibration map between the actual moisture values and their corresponding estimated permittivity change percentage on the wet basis was found. A linear mapping proved to be sufficient considering the measurement data. This mapping was obtained as

$$\Delta\epsilon_{\mathrm{w}} = (0.745 \pm 0.083)M - 1.538 \pm 3.660. \tag{15}$$

Figure 11 shows the measured data, the fitted curve, and the 95% confidence interval for the stationary experiments. The mapping (15) was used to find the estimated moisture distributions from the stationary experiments illustrated in Fig. 12. In this figure, the actual locations of the wet pieces are indicated in every subfigure with a red rectangle accompanied by a corresponding label (P1, P2, and P3). The actual moisture percentage, M, of every piece in these experiments and its estimated value, M_{e}, are given in Table I. The relative moisture estimation error, e_{M}, is also computed for every piece and indicated in Table I for a more straightforward evaluation of the results. The relative estimation error was determined as

$$e_{\mathrm{M}} = \frac{|M - M_{\mathrm{e}}|}{M} \times 100, \tag{16}$$

where M_{e} is the estimated moisture percentage.

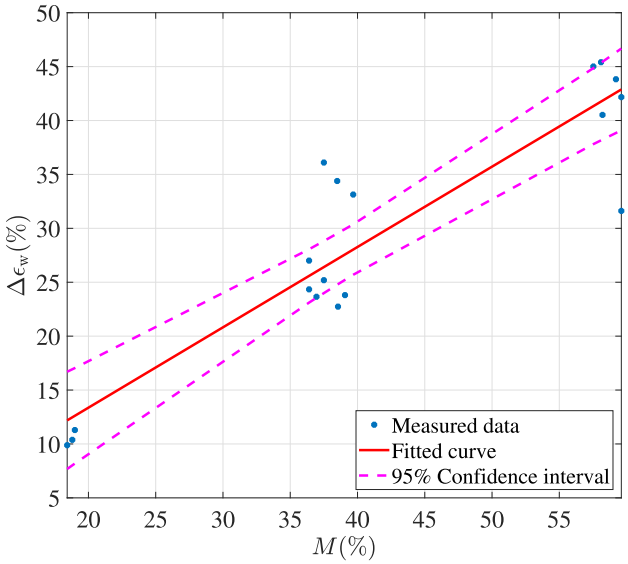

Fig. 11. The mapping between the wet basis moisture percentage and the wet basis permittivity change percentage in the stationary experiments.

TABLE I
MOISTURE PERCENTAGE, M, THE AVERAGE ESTIMATED MOISTURE, M_e, AND THE RELATIVE MOISTURE ESTIMATION ERROR, e_M, OF EVERY PIECE IN THE STATIONARY EXPERIMENTS

Experiment	Piece	M(%)	M_e (%)	e_M (%)
Experiment 1	P1	59.2	59.7	0.8
	P2	36.4	37.9	4.1
	P3	37.0	33.6	9.2
Experiment 2	P1	58.1	61.4	5.7
	P2	59.6	56.8	4.7
	P3	36.4	34.4	5.5
Experiment 3	P1	57.5	61.4	6.8
	P2	58.2	55.7	4.3
	P3	59.6	43.3	27.3

Figure 12a shows a case where P1 has more moisture than P2 and P3, while those two pieces have almost the same moisture. As shown in this figure, all the moisture locations are identified correctly, and the moisture estimations are higher in the P1 location than in the other two places. The higher average moisture estimate of P1 can also be seen from the values of M_e in Table I. As seen from this table, the average moisture estimate of all three pieces follows their actual values. The estimation error in this experiment varies from 0.8% to 9.2%.

In the second experiment, the moisture content of P2 was increased to reach the same amount as P1. The estimated moisture distribution for P2 in Fig. 12b clearly shows the increase in moisture compared to the estimated moisture distribution in Experiment 1. Moreover, the information given in Table I shows that the average estimated moisture for P2 has increased in Experiment 2 compared to Experiment 1. In this experiment, P3 had the least average estimated moisture as it contained the lowest amount of water among all the pieces.

The third experiment studied a case where the moisture level of P3 was increased compared to the previous experiments. In this experiment, all the pieces had almost the same amount of moisture. Figure 12c displays the reconstruction result of this measurement. As shown in this figure and can be followed from Table I, the first and second moisture locations are identified correctly. However, there is a position error in identifying P3, probably due to water leakage from P3 to the neighboring area. As the third experiment was done right after the first two experiments, and it involved more moisture, the amount of water moving to the surroundings could be higher. It can be seen from the estimation errors shown in Table I that the estimation errors for P1 and P2 are 6.8% and 4.3%, respectively, while it is 27.3% for P3 for the possible reasons mentioned. The average estimation error for all the stationary experiments was 7.6%. Although the relatively high estimation error for P3 in the third experiment raised the average estimation error, the error is satisfactory and close to process control requirements.

B. Reconstruction Results of Dynamic Measurements

In this section, the reconstruction results of the dynamic experiments where the foam was continually moving on the conveyor belt are discussed. Each frame of measurements in ECT takes almost 720 ms. As the speed of the conveyor belt is relatively slow (20-40 cm/min), the measurement time and the reconstruction time are short enough and make it possible to use these measurements in a closed-loop moisture controller unit. In the following experiments, the sample time was taken as 1 s.

The sample foam tested in these experiments is shown in Fig. 9. While the foam passed through the electrode plane of the ECT sensor, 2D reconstructions were calculated at each time instant. As mentioned in Section IV-B, it was assumed that the permittivity in the foam moving direction is constant. With this assumption, mostly the cross-section of the target foam under the electrode plane was reconstructed. As the electrodes were larger than the wet pieces, there were some effects from the neighboring area to that cross-section. A mapping between the actual moisture of pieces in these experiments and the normalized estimated permittivity change, $\Delta\epsilon_w$, was obtained as

$$\begin{aligned}\Delta\epsilon_w = {} & (0.002 \times 10^{-1} \pm 2.938 \times 10^{-4})M^3 \\ & + (-0.021 \pm 0.040)M^2 + (1.087 \pm 1.693)M \\ & - 10.672 \pm 21.441. \end{aligned} \tag{17}$$

The measured data, the fitted curve, and the 95% confidence interval for the mapping in the dynamic experiments are shown in Fig. 13.

In the first experiment, the sensor performance was evaluated while the foam moved on a conveyor belt with a speed of 40 cm/min. In this experiment, the actual microwave heating effect was not considered because the heating would have resulted in the evaporation of the moisture in the foam and made it difficult to validate the reconstruction results.

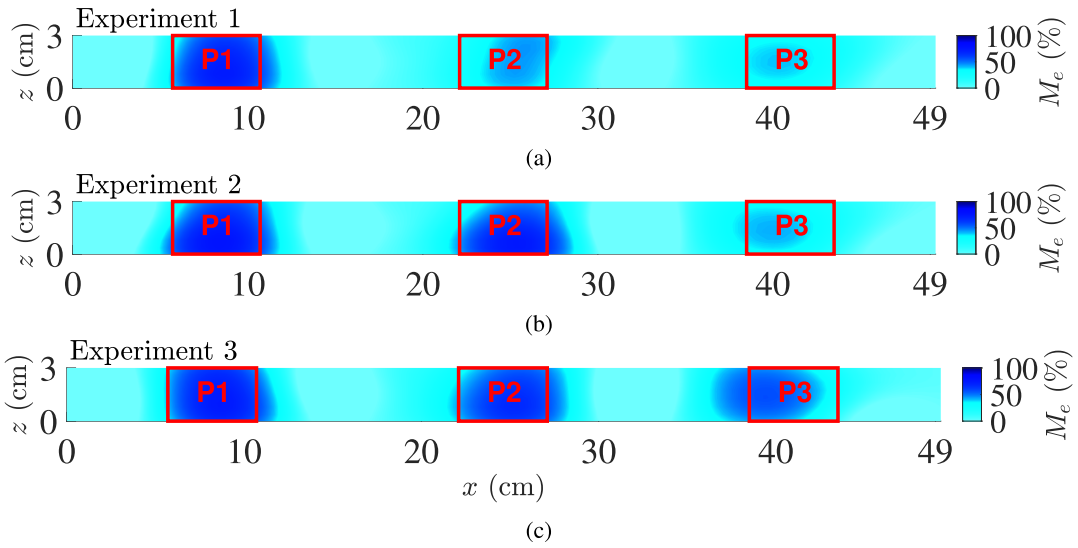

Fig. 12. Reconstruction results from the stationary experiments. (a) The first experiment in which P1 has the highest moisture level while P2 and P3 have almost the same moisture level. (b) The second experiment in which P1 and P2 have nearly the same moisture while P3 has the lowest moisture level. (c) The third experiment with all three pieces having almost the same moisture level.

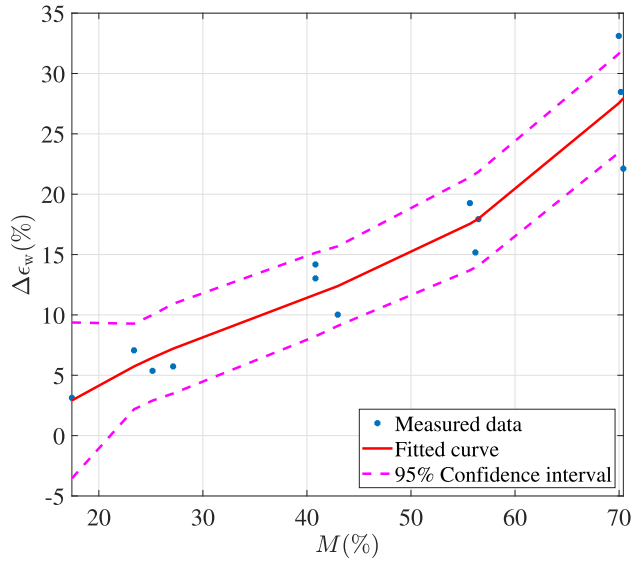

Fig. 13. The mapping between the wet basis moisture percentage and the wet basis permittivity change percentage in the dynamic experiments.

Therefore, in the first and third experiments, the microwave sources were off, and only the belt speed factor was examined.

Figure 14 shows the 2D reconstructions at nine different time instants, in which each row of the sample foam was precisely in the middle of the electrode planes. As the electrode plane had a 100 mm length, there were several time instants when each cross-section of the foam was under this plane. In this figure, only the middle cross-section is demonstrated, and the rest are not shown. The time variable, t, shows the time passed from the beginning of the experiment. Here, $t = 0$ is when the foam just entered the sensor frame. As in the stationary case, the red rectangles indicate the actual locations of the pieces. Since the foam was moving on the conveyor belt in the y-direction, there were some small movements to the sides in the x-direction, resulting in small errors between the actual and estimated locations of the pieces.

TABLE II
THE DISTANCE BETWEEN THE PIECES (FROM SIDE TO SIDE) IN EACH EVEN ROW OF THE SAMPLE FOAM USED IN THE DYNAMIC EXPERIMENTS

Row	Row 2	Row 4	Row 6	Row 8
Pieces	P2 & P3	P5 & P6	P8 & P9	P11 & P12
Distance (mm)	50	90	140	190

All the 2D reconstructions from the whole experiment were stacked together to create a 3D visualization of these experiments, as shown in Fig. 15. Since the pieces in this experiment had different moisture levels, four thresholds in the estimated moisture distribution were selected to show the variation in the moisture estimates more clearly. The location, moisture content, and the size of the pieces in the sample foam were the three factors that their effects were studied on the reconstructions.

The first factor to study was the sizes of the pieces in the sample foam. The pieces were in two different sizes. The ones on the odd rows were 50 mm in width, while the pieces on the even rows were 80 mm in width. The length and the thickness of all the pieces were 50 mm and 30 mm, respectively. As the reconstruction in Fig. 15 shows, the ECT sensor can identify moisture in both sizes. Since the wavelength of the microwaves in our application is 120 mm, a spatial resolution comparable to the half wavelength, 60 mm, is sufficient for process control. Therefore, the ECT sensor can identify the moisture in any reachable location in this application.

The second subject to study was the distance between the wet pieces. As seen in Fig. 9, two pieces are in each even row, and different distances are considered between these pieces to evaluate the sensor resolution. The idea was to see if the ECT sensor can detect these two pieces in separate locations or

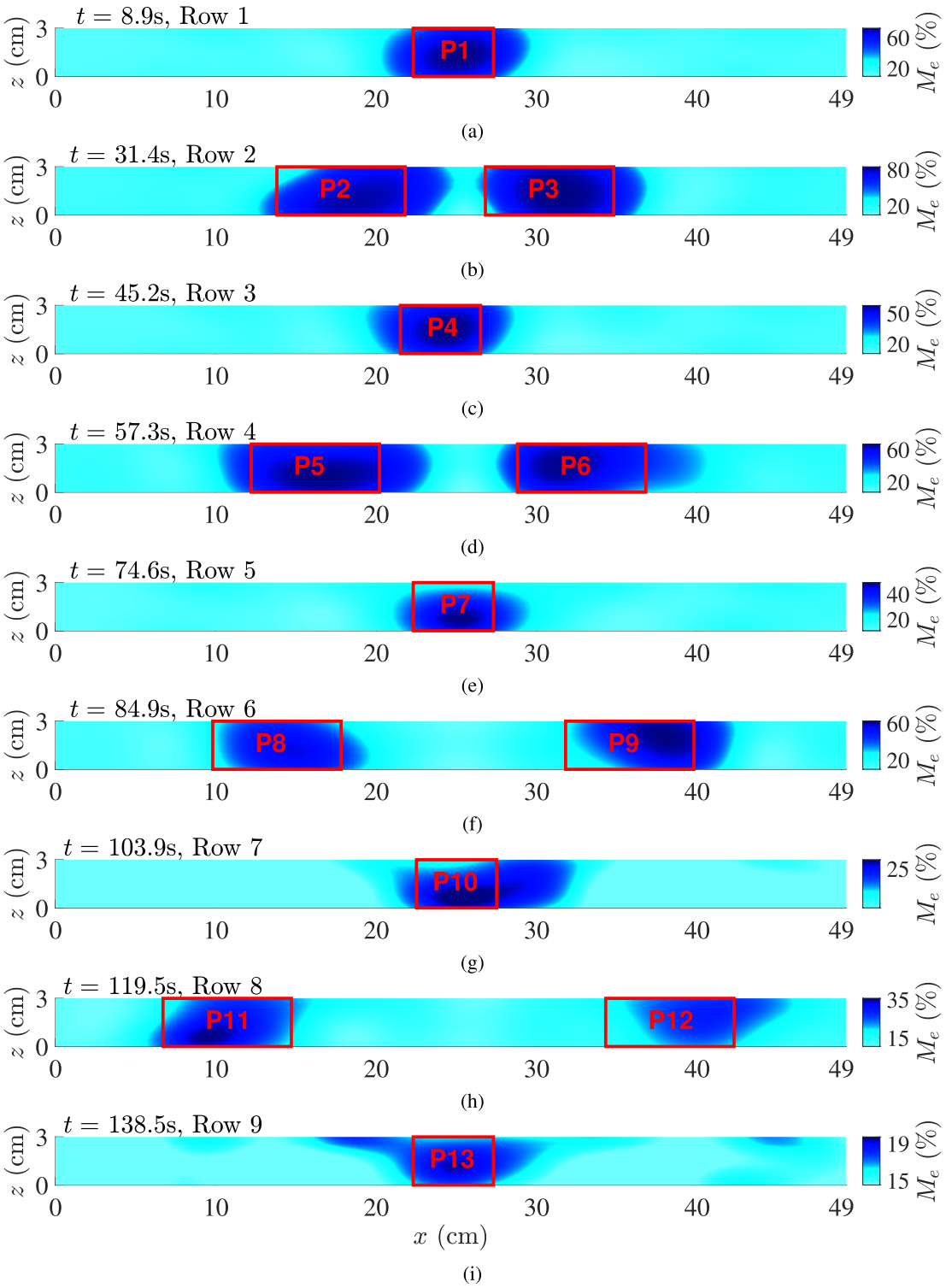

Fig. 14. 2D reconstruction results from the first dynamic experiment with the belt speed of 40 cm/min while the microwave sources were off. Each of the reconstructions is related to one of the rows in the sample foam when they passed through the electrode plane.

see them as a single moisture object. The label of the pieces located in each even row and their distance from each other are given in Table II.

The pieces in Row 2 had the least distance, while at the same time, they had the most amount of moisture compared to the other pieces. Based on the reconstructions in Fig. 15, although there is some reconstructed moisture in the connecting domain of these two pieces, the ECT sensor has identified two separate moisture locations on this row. Figure 14b also shows the separate reconstructed moisture locations clearly. Identifying moisture in the connecting domain was because of spreading water from the wet pieces to the neighboring area.

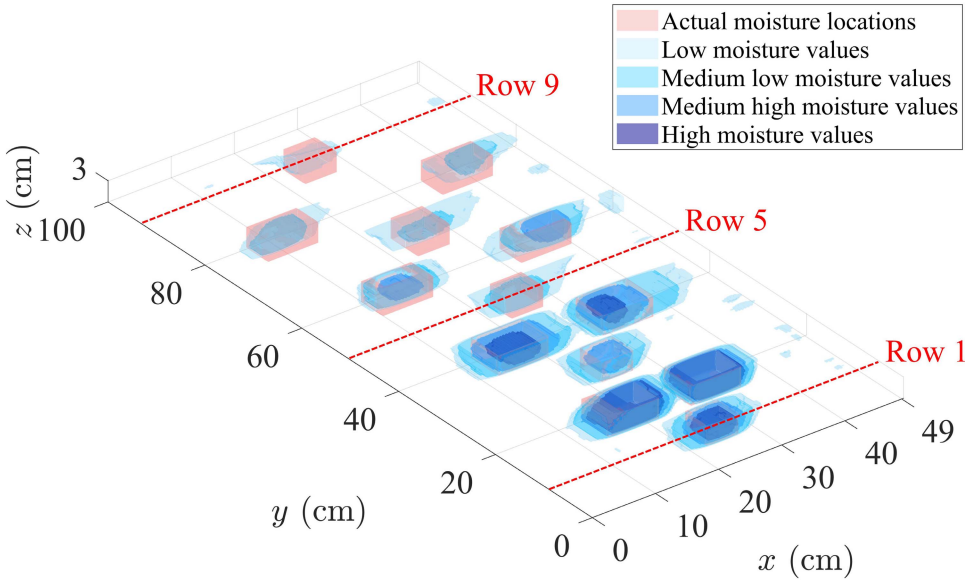

Fig. 15. 3D visualization of the first dynamic experiment with a conveyor belt speed of 40 cm/min while the microwave sources were off.

TABLE III
MOISTURE PERCENTAGES M, THE AVERAGE ESTIMATED MOISTURE M_e, AND THE MOISTURE ESTIMATION ERROR, e_M, OF EVERY PIECE IN THE DYNAMIC EXPERIMENTS

P	P1	P2	P3	P4	P5	P6	P7	P8	P9	P10	P11	P12	P13
M (%)	70.4	70.2	70.0	56.2	55.7	56.5	43.0	40.8	40.8	27.1	23.4	25.2	17.4
M_e (%)	61.8	66.7	72.5	49.9	57.8	55.0	35.6	43.8	45.5	23.5	27.0	22.8	17.8
e_M (%)	12.2	5.0	3.5	11.2	3.8	2.6	17.2	7.3	11.6	13.4	15.5	9.5	2.5

The resolution of the ECT sensor and the smoothness assumption in the reconstruction algorithm might be the other reasons for the moisture reconstruction in the adjacent regions. Edge preserving priors could reduce this effect; however, the moisture locations do not have sharp edges in practice. In all the other even rows, the pieces are also identified in entirely separate places. In conclusion, it can be said that if the moisture locations are almost 50 mm apart, the ECT sensor can detect them as separate locations. Considering the microwave wavelength, this is an acceptable and sufficient distance.

The third factor to study in this experiment was the moisture content of the sample foam pieces. This experiment evaluated the ECT sensor sensitivity to different amounts of moisture contents. The added water to the pieces was decreased from the first row to the last row, as can be read from Table III. The moisture values in this table are approximately correct as the water starts to evaporate during the experiment, and there will be slightly less moisture than at the beginning.

The reconstruction in Fig. 15 clearly shows the different moisture levels in all 13 pieces. The last piece, P13, had the least amount of moisture, and only the minimum level among the four chosen thresholds of the estimated moisture values can be seen in this location. The first three pieces in the sample foam, on the other hand, had the largest moisture content, which is also shown in the reconstruction. The average estimated moisture and the moisture estimation error for all the 13 pieces are noted in Table III. The estimation errors for several pieces were adequately small while it was substantial for the rest of them. The large estimation error could be due to water moving to the neighboring area or small foam movements to the sides (x-direction). The average estimation error in this experiment was 8.9%. The results showed that the ECT sensor could identify the moisture amount from 17% to 70%. Although the detectable moisture range can be wider, it is far broader than the requirements of our application.

In the actual process, the ECT sensor is working quite close to the microwave oven. As it is an open oven, there is always some microwave leakage, possibly disturbing the measurements. Therefore, we needed to operate the ECT sensor while the microwave sources were on and study the effect on the moisture estimates. Experiment 2 evaluated the sensor performance with the same belt speed and the same sample foam as Experiment 1. The only difference was that the microwave sources worked with their 25% maximum power in this experiment. Since the actual foam moisture needed to stay constant in this study to validate the estimations, the microwave sources were activated only when the foam had already passed the oven and entered the microwave filter area where the microwave sources could not heat the foam. The results proved that the ECT sensor could work near the microwave oven without any visible effects on the reconstructions. Since the reconstruction results were similar to the reconstructions from Experiment 1, they have not been illustrated anymore.

In the last experiment, the effects of a different belt speed on the moisture estimates were studied. In this experiment,

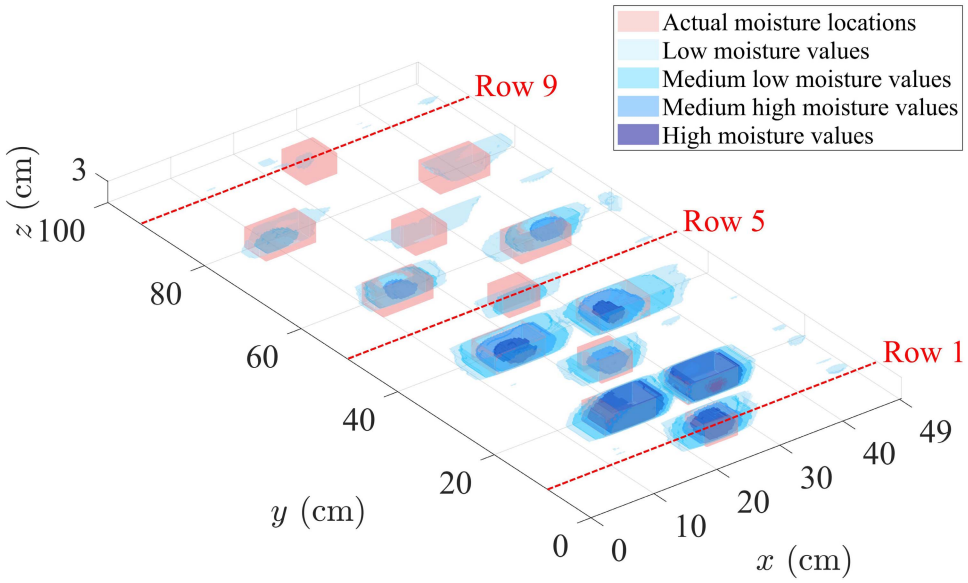

Fig. 16. 3D visualization of the third dynamic experiment with a conveyor belt speed of 20 cm/min while the microwave sources were off.

the belt speed was set to 20 cm/min. The 3D visualization from the results of this experiment is demonstrated in Fig. 16. Since this was the last experiment and took a long time as the belt speed was low, some of the foam moisture was already evaporated. Comparing Fig. 15 and Fig. 16, it can be seen that, for instance, P13 has less moisture in the last experiment compared to the first one. Nonetheless, all moisture locations are identified correctly, and the results show that the ECT sensor has good performance with both belt speeds of 20 cm/min and 40 cm/min.

VI. Conclusion

In this paper, we studied the performance of our designed ECT sensor in estimating the moisture distribution of polymer foam in two states of being stationary and moving on a conveyor belt. The reconstruction algorithm computes the permittivity change distribution of the foam. However, the material permittivity strongly correlates with its moisture, so using a calibration map, the moisture distribution was estimated in all experiments. First, three different stationary experiments were conducted, which showed the excellent performance of the ECT in detecting the moisture locations and distinguishing different moisture percentages. The average estimation error in the stationary experiments was 7.6%. Then, in the dynamic experiments, the measurements were done while the foam was moving on a conveyor belt. In these experiments, two different belt speeds were chosen, and the effect of the microwave power (without heating) was studied. The results showed very acceptable performance from the ECT sensor in the usual working belt speeds. In addition, the microwave power did not affect the ECT sensor signal and, therefore, the reconstructions.

In the dynamic experiments, the size of the moisture locations, the distance between them, and the moisture level in those locations were studied. The experimental results showed that the ECT sensor could easily detect small moisture objects with an area of 50 mm $\times$ 50 mm. The results also showed that the minimum distance in which the ECT sensor could distinguish two separate moisture locations was 50 mm. This distance was determined at a high-level moisture content (approximately 70%), while the distance can be smaller between the pieces with lower moisture content since the water moving to the surrounding area will be less. Moreover, the moisture percentages were estimated with reasonable accuracy. However, estimation error in some cases was large, and the average estimation error in the dynamic experiments was 8.6%.

The moisture estimation error should be reduced to nearly 5% so that the moisture estimates will be useful for moisture control. One solution to reduce the estimation error is to enhance the conveyor belt equipment and prevent foam from moving to the sides. It also should be noted that in practice, the foam moisture content after the drying process is lower than the moisture levels studied in our experiments. Removing the higher level moisture data and increasing the number of samples with the lower moisture level in the calibration may also reduce the moisture estimation error.

The experimental results, in general, proved that the accuracy and the resolution of the ECT sensor are satisfactory, and this sensor is a suitable candidate for process control, which is one of the motivations of this paper. The measurement time is short enough (in this study, 720 ms), and the reconstruction time also takes less than a second. Therefore, the measurements can be easily used in a closed-loop moisture control as the foam moisture feedback.

Acknowledgment

The authors would like to thank Dr. Tuomo Savolainen from the Department of Applied Physics, University of Eastern Finland, for building the ECT sensor. They would also like to thank Volker Nuss and Dominik Neumaier from the HEPHAISTOS Laboratory, Karlsruhe Institute of Technology, Germany.

REFERENCES

[1] P. Rattanadecho and N. Makul, "Microwave-assisted drying: A review of the state-of-the-art," *Drying Technol.*, vol. 34, no. 1, pp. 1–38, Jan. 2016.

[2] M. Bartholme, G. Avramidis, W. Viöl, and A. Kharazipour, "Microwave drying of wet processed wood fibre insulating boards," *Eur. J. Wood Wood Products*, vol. 67, no. 3, pp. 357–360, Aug. 2009.

[3] G. Link and V. Ramopoulos, "Simple analytical approach for industrial microwave applicator design," *Chem. Eng. Process. Process Intensification*, vol. 125, pp. 334–342, Mar. 2018.

[4] Z. Li, G. S. V. Raghavan, and V. Orsat, "Temperature and power control in microwave drying," *J. Food Eng.*, vol. 97, no. 4, pp. 478–483, Apr. 2010.

[5] G. Cuccurullo, L. Giordano, D. Albanese, L. Cinquanta, and M. Di Matteo, "Infrared thermography assisted control for apples microwave drying," *J. Food Eng.*, vol. 112, no. 4, pp. 319–325, Oct. 2012.

[6] J. I. Lombraña, R. Rodríguez, and U. Ruiz, "Microwave-drying of sliced mushroom. Analysis of temperature control and pressure," *Innov. Food Sci. Emerg. Technol.*, vol. 11, no. 4, pp. 652–660, Oct. 2010.

[7] Z. Li, G. S. V. Raghavan, and N. Wang, "Carrot volatiles monitoring and control in microwave drying," *LWT Food Sci. Technol.*, vol. 43, no. 2, pp. 291–297, Mar. 2010.

[8] T. Rymarczyk and J. Sikora, "Applying industrial tomography to control and optimization flow systems," *Open Phys.*, vol. 16, no. 1, pp. 332–345, Jun. 2018.

[9] H. Tabe, S. Simons, J. Savery, R. West, and R. Williams, "Modelling of multiphase processes using tomographic data for optimisation and control," in *Proc. 1st World Congr. Ind. Process Tomogr.*, Buxton, U.K., Apr. 1999, pp. 1–6.

[10] A. R. Ruuskanen, A. Seppänen, S. Duncan, E. Somersalo, and J. P. Kaipio, "Using process tomography as a sensor for optimal control," *Appl. Numer. Math.*, vol. 56, no. 1, pp. 37–54, Jan. 2006.

[11] T. Lahivaara, R. Yadav, G. Link, and M. Vauhkonen, "Estimation of moisture content distribution in porous foam using microwave tomography with neural networks," *IEEE Trans. Comput. Imag.*, vol. 6, pp. 1351–1361, Sep. 2020.

[12] H. Zhu, T. Gulati, A. K. Datta, and K. Huang, "Microwave drying of spheres: Coupled electromagnetics-multiphase transport modeling with experimentation. Part I: Model development and experimental methodology," *Food Bioproducts Process.*, vol. 96, pp. 314–325, Oct. 2015.

[13] T. Gulati, H. Zhu, A. K. Datta, and K. Huang, "Microwave drying of spheres: Coupled electromagnetics-multiphase transport modeling with experimentation. Part II: Model validation and simulation results," *Food Bioproducts Process.*, vol. 96, pp. 326–337, Oct. 2015.

[14] W. M. Cheng, G. S. V. Raghavan, M. Ngadi, and N. Wang, "Microwave power control strategies on the drying process II. Phase-controlled and cycle-controlled microwave/air drying," *J. Food Eng.*, vol. 76, no. 2, pp. 195–201, Sep. 2006.

[15] C. Kumar, M. U. H. Joardder, T. W. Farrell, and M. A. Karim, "Investigation of intermittent microwave convective drying (IMCD) of food materials by a coupled 3D electromagnetics and multiphase model," *Drying Technol.*, vol. 36, no. 6, pp. 736–750, Apr. 2018.

[16] P. Chen and P. S. Schmidt, "An integral model for drying of hygroscopic and nonhygroscopic materials with dielectric heating," *Drying Technol.*, vol. 8, no. 5, pp. 907–930, Jan. 1990.

[17] B. Adu and L. Otten, "Diffusion characteristics of white beans during microwave drying," *J. Agricult. Eng. Res.*, vol. 64, no. 1, pp. 61–69, May 1996.

[18] V. Rimpiläinen, L. M. Heikkinen, and M. Vauhkonen, "Moisture distribution and hydrodynamics of wet granules during fluidized-bed drying characterized with volumetric electrical capacitance tomography," *Chem. Eng. Sci.*, vol. 75, pp. 220–234, Jun. 2012.

[19] A. Voss, N. Hänninen, M. Pour-Ghaz, M. Vauhkonen, and A. Seppänen, "Imaging of two-dimensional unsaturated moisture flows in uncracked and cracked cement-based materials using electrical capacitance tomography," *Mater. Struct.*, vol. 51, no. 3, p. 68, Jun. 2018.

[20] A. Voss, P. Hosseini, M. Pour-Ghaz, M. Vauhkonen, and A. Seppänen, "Three-dimensional electrical capacitance tomography—A tool for characterizing moisture transport properties of cement-based materials," *Mater. Des.*, vol. 181, Nov. 2019, Art. no. 107967.

[21] W. Wang, K. Zhao, P. Zhang, J. Bao, and S. Xue, "Application of three self-developed ECT sensors for monitoring the moisture content in sand and mortar," *Construct. Building Mater.*, vol. 267, Jan. 2021, Art. no. 121008.

[22] H. G. Wang, P. R. Senior, R. Mann, and W. Q. Yang, "Online measurement and control of solids moisture in fluidised bed dryers," *Chem. Eng. Sci.*, vol. 64, no. 12, pp. 2893–2902, Jun. 2009.

[23] P. Pan, T. P. McDonald, B. K. Via, J. P. Fulton, and J. Y. Hung, "Predicting moisture content of chipped pine samples with a multi-electrode capacitance sensor," *Biosyst. Eng.*, vol. 145, pp. 1–9, May 2016.

[24] M. Hosseini, A. Kaasinen, G. Link, T. Lähivaara, and M. Vauhkonen, "LQR control of moisture distribution in microwave drying process based on a finite element model of parabolic PDEs," *IFAC-PapersOnLine*, vol. 53, no. 2, pp. 11470–11476, 2020.

[25] E. Somersalo, M. Cheney, and D. Isaacson, "Existence and uniqueness for electrode models for electric current computed tomography," *SIAM J. Appl. Math.*, vol. 52, no. 4, pp. 1023–1040, Aug. 1992.

[26] A. Voss, "Imaging moisture flows in cement-based materials using electrical capacitance tomography," Ph.D. dissertation, Dept. Appl. Phys., Univ. Eastern Finland, Kuopio, Finland, 2020.

[27] P. J. Vauhkonen, M. Vauhkonen, T. Savolainen, and J. P. Kaipio, "Three-dimensional electrical impedance tomography based on the complete electrode model," *IEEE Trans. Biomed. Eng.*, vol. 46, no. 9, pp. 1150–1160, 1999.

[28] D. Watzenig and C. Fox, "A review of statistical modelling and inference for electrical capacitance tomography," *Meas. Sci. Technol.*, vol. 20, no. 5, May 2009, Art. no. 052002.

[29] M. Soleimani and W. R. B. Lionheart, "Nonlinear image reconstruction for electrical capacitance tomography using experimental data," *Meas. Sci. Technol.*, vol. 16, no. 10, p. 1987, 2005.

[30] W. Q. Yang and L. Peng, "Image reconstruction algorithms for electrical capacitance tomography," *Meas. Sci. Technol.*, vol. 14, no. 1, pp. R1–R13, Jan. 2003.

[31] J. Lei, S. Liu, Z. Li, M. Sun, and X. Wang, "A multi-scale image reconstruction algorithm for electrical capacitance tomography," *Appl. Math. Model.*, vol. 35, no. 6, pp. 2585–2606, Jun. 2011.

[32] J. Kaipio and E. Somersalo, *Statistical and Computational Inverse Problems*, vol. 160. New York, NY, USA: Springer, 2006.

[33] A. Lipponen, A. Seppänen, and J. Kaipio, "Electrical impedance tomography imaging with reduced-order model based on proper orthogonal decomposition," *J. Electron. Imag.*, vol. 22, no. 2, May 2013, Art. no. 023008.

Marzieh Hosseini received the M.Sc. degree in electrical engineering–control systems from the Qazvin Islamic Azad University, Qazvin, Iran, in 2015. She is currently pursuing the Ph.D. degree with the Department of Applied Physics, University of Eastern Finland. She is with the TOMOCON Program, a Marie Skłodowska-Curie European training network studying the innovative idea of combining tomographic sensors into control systems. Her research interests include optimal control, process tomography, and system identification.

Anna Kaasinen received the Ph.D. degree in applied physics from the University of Eastern Finland, Kuopio, Finland, in 2013. She is currently a University Lecturer in mathematics with the Department of Applied Physics, University of Eastern Finland. Her research interests include optimal control, process control, and process tomography.

Guido Link received the Dipl.-Phys. and Dr.rer.nat. degrees in physics from Technical University Karlsruhe, Germany, in 1990 and 1993, respectively. His diploma thesis and graduate research were devoted to the frequency and temperature dependent dielectric characterization of low loss ceramics and ionic crystals. Since 1993, he has been working with the Karlsruhe Institute of Technology (former Forschungszentrum Karlsruhe), Germany, in the field of high power microwave and millimeter-wave processing of materials, as a Team Leader at the Institute for Pulsed Power and Microwave Technology. His research interests include dielectric measurements, design, and simulation of microwave systems and processes, microwave-assisted sintering, curing of polymer composites, additive manufacturing, and plasma chemistry.

Timo Lähivaara received the M.Sc. degree from the University of Kuopio, Kuopio, Finland, in 2006, and the Ph.D. degree from the University of Eastern Finland, Kuopio, in 2010.

He is currently a Senior Researcher with the Department of Applied Physics, University of Eastern Finland. His research interests include computational wave problems and remote sensing.

Marko Vauhkonen received the Ph.D. degree in physics from the University of Kuopio, Finland, in 1997. After graduation, he worked as a Researcher and the Research Director of the University of Kuopio, Germany, in 2006. He worked as a Marie-Curie Research Fellow at Philips Research GmbH, Aachen, for two years. From 2008 to 2009, he worked as a CTO at Numcore Ltd., a spin-off company, until starting as a Professor with the Department of Applied Physics, University of Kuopio (currently University of Eastern Finland), in 2009. He has published more than 100 scientific journal articles. His research interests include inverse problems, time-varying reconstruction, process tomography, and medical imaging, such as PET, SPECT, and MRI.